실험을 통한 모션제어기의 특성비교

Characteristics Comparison of Motion Controllers through Experiments

정 승 현, 왕 준, 한 창 욱, 박 정 일*
(Seung Hyun Jung, Jun Wang, Chang Wook Han and Jung-Il Park)

Abstract : Through the motion control experiment using Industrial Emulator(Model 220 by ECP), the performance comparison of three kinds of controllers such as PID, RIC and LQR was carried out. It was shown that RIC has the best performance in the presence of disturbances such as step one, sinusoidal one and Coulomb friction for the rigid body. LQR using feedback state variables has the best tracking performance for the flexible body. The performance of PID controller is low compared to other controllers, but the design process is simple. The most advanced controller is LQR. In order to attenuate disturbance, an additional state observer should be used to estimate it, making more complex control system. RIC lies between PID and LQR in view of complexity of design. Even though RIC is not complicated, it has good disturbance rejection ability and less tracking error. By considering these aspects, the RIC is suggested as high precision controller to be used in motion control system.

Keywords : disturbance rejection, motion control, LQR, PID, RIC(Robust Internal-loop Compensator)

I. INTRODUCTION

The motion controller is used to make motion action of the industrial automation system. Many researches have been devoted to obtain the desired dynamic performance of electromechanical systems with servo motors. The main issue in designing precision positioning systems such as factory automation, high-tech computer hard disk drives, and semiconductor chip mounter/wire bonder is how to achieve high-speed/high-accuracy performance.

In designing a robust controller for a system in the presence of uncertainty and disturbance, the first requirement is to achieve the robustness properties on the uncertainties including external disturbance, variations of the system parameters, modeling uncertainties, and etc., and the second one is to obtain the performance specifications for given tasks. Many advanced controller design methods have been proposed to meet these requirements. The Disturbance Observers(DOB)[1,2], an Adaptive Robust Control(ARC)[3], Active Disturbance Rejection Controller (ADRC)[4], state observer design for reduction torsional vibration[5], robust motion controller design[6] are good examples. These methods commonly require the design of two loop structures. One is to design the internal-loop compensator for robustness, the other is to design the external-loop controller for desired performance specifications. In such scheme, the internal-loop compensator generates corrective control inputs to reject equivalent disturbance as much as possible to force the actual system to become a given nominal model, where the equivalent disturbance is defined as sum of external disturbance signals and all possible signals due to the differences between the actual plant and nominal model such as modeling uncertainty and parameter variations. Thus, the actual plant with such an internal-loop compensator can be regarded as a nominal model if the internal-loop compensator works well. On the other hand, the external-loop controller is designed to enhance overall system performance, where controller design is carried out for the nominal model.

In this paper, the comparison experiments using Industrial Emulator made by ECP were conducted to analyze the accuracy and robustness of three kinds of controllers for positioning system in the presence of disturbance. In Section II, the disturbance compensation algorithms used in comparison experiments are reviewed. In Section III, the experiment system, so called Industrial Emulator, introduced to verify the performance of each motion controller is described. In Section IV, PID(Proportional Integral Derivative), RIC(Robust Internal-loop Compensator) and LQR(Linear Quadratic Regulator) controllers are designed for high-accuracy positioning systems for rigid body, also these experiments using ECP to compare their performance are carried out. PID, RIC and LQR are also designed for flexible body. Finally, conclusions will be followed.

II. REVIEW OF CONTROLLERS TO APPLY MOTION CONTROL

In this section, the motion control theories used to remove the disturbance are described. The fundamental concepts of servo motion control is using servo systems to improve transient response time, reduce the steady state error and reduce influence of the disturbance.

Servo motion control usually has two fundamental classes. The first class deals with command tracking. The typical commands in rotary motion control are position, velocity, acceleration and torque. The second one addresses the disturbance rejection characteristics of the system. The goal of the servo control systems is how to combine both these points of servo control to provide the best overall performance.

The dynamic equation of general servo system can be expressed as

$$J\ddot{y} + c\dot{y} + F_r(\dot{y}) - d_{ex} = u \tag{1}$$

where J is the inertia, c is the damping coefficient, u is the control input, y is the output of interest, $F_r(\dot{y})$ is the friction term including static friction and Coulomb friction, d_{ex} is the uncertain external disturbance whose magnitude is bounded. Tracking error is defined as

$$e = y_d - y \tag{2}$$

where y_d is a desired trajectory.

* 책임저자(Corresponding Author)
논문접수 : 2007. 7. 25., 채택확정 : 2008. 8. 13.
정승현, 왕준, 박정일 : 영남대학교 전자정보공학부
(shj@kotmi.re.kr/oldwolf_wang@hotmail.com/jipark@yu.ac.kr)
한창욱 : 동의대학교 전기공학과(cwhan@deu.ac.kr)

Among various controllers, three kinds of controllers such as the most simple and conventional PID controller, the RIC equivalent to DOB which has been most widely studied in view of disturbance rejection, and the LQR which is the most advanced modern controller are introduced for the performance comparison of motion control.

1. PID control

The PID is the most common form of feedback controller. The control input by PID controller is described by:

$$u(t) = K_P e(t) + K_i \int_0^t e(\tau)d\tau + K_d \frac{de(t)}{dt} \tag{3}$$

where $e(t)$ is the error, K_p is proportional gain, K_i is integral gain, and K_d is derivative gain. Rewriting (3) in s-domain,

$$\frac{U(s)}{E(s)} = K_p + \frac{K_i}{s} + K_d s \tag{4}$$

2. Linear Quadratic Regulator(LQR)

The plant represented in state space is given by,

$$\dot{x} = Ax + Bu \tag{5}$$

The optimal control input is given by,

$$u(t) = -Kx(t) \tag{6}$$

where K is the gain matrix, which is chosen so that the following performance index is minimized.

$$J = \int_0^\infty \left(x^T Q x + u^T R u \right) dt \tag{7}$$

where Q, R are a positive-definite matrices. ($u^T Ru$) term accounts for the expenditure of the energy of the control signals. The weighting matrices Q and R determine the relative importance of the error and the expenditure of this energy.

Solving the LQR problem, Riccati matrix differential equation is obtained as

$$-\dot{S} = A^T S + SA - SBR^{-1}B^T S + Q \tag{8}$$

$S(t)$ can be obtained by backwards integration of this equation. The closed loop optimal control law can be found by

$$u = -R^{-1}B^T Sx \tag{9}$$

3. Robust Internal-loop Compensator(RIC)

Recently, a robust controller, Robust Internal-loop Compensator(RIC) by Kim B. K. and Chung W. K[7], is designed for the system in the presence of uncertainty and disturbance. It was known that RIC is equivalent to the conventional DOB structure shown in Fig.

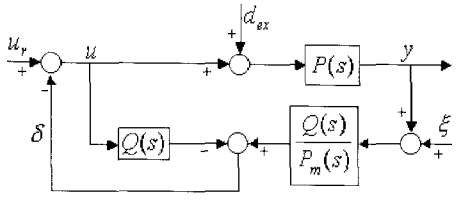

그림 1. DOB의 구조.

Fig. 1. Structure of the DOB

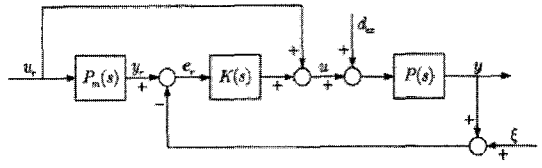

그림 2. RIC의 일반적 구조.

Fig. 2. A generalized framework of RIC.

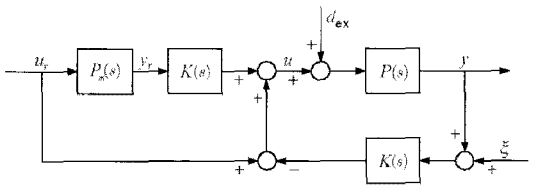

그림 3. RIC의 등가구조.

Fig. 3. A equivalent framework of RIC.

1. Using the low-pass filter $Q(s)$ and the inverse of a nominal model, the DOB estimates the disturbance and the estimated signal utilized for disturbance compensation.

A generalized framework of RIC is shown in Fig. 2. Fig. 2 can be transformed as Fig. 3.

Comparing Fig. 2 with Fig. 3, the following equations are obtained.

$$Q(s) = \frac{P_m(s)K(s)}{1+P_m(s)K(s)}, \quad K(s) = \frac{Q(s)}{P_m(s)(1-Q(s))} \tag{10}$$

The RIC structure of Fig. 3 can be transformed equivalently to a structure of DOB shown in Fig. 4.

From the block diagram in Fig. 4, the input-output relationship from the external disturbance d_{ex} to the plant output can be expressed as

$$G_{d_{ex}d} = \frac{P(s)P_m(s)(1-Q(s))}{P_m(s) + (P(s) - P_m(s))Q(s)} \tag{11}$$

Below the cutoff frequency of $Q(s)$, $Q(s) \approx 1$ is achieved. Hence $G_{d_{ex}y} \approx 0$ is obtained from (11). This indicates that the disturbances are attenuated and mismatch between plant and reference model is compensated in the low frequency region.

In order to design a robust motion controller using RIC framework, consider the following reference model for general positioning system of (1),

$$J_m \ddot{y} + c_m \dot{y} = u + d_{eq} \tag{12}$$

where J_m and c_m are the reference values of inertia J and viscous

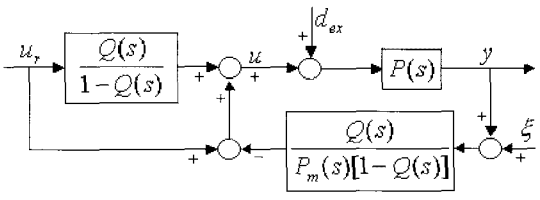

그림 4. Q함수를 사용한 RIC의 등가구조.

Fig. 4. Equivalent structure of RIC using Q function.

friction c, respectively.

$$d_{eq} = (J_m - J)\ddot{y} + (c_m - c)\dot{y} - F_r(\dot{y}) + d_{ex} \quad (13)$$

And the reference control input that can stabilize the reference model given by (12) can be chosen as

$$u = J_m \ddot{y} + c_m \dot{y}_r \quad (14)$$

The reference model $P_m(s)$ is described by

$$P_m(s) = \frac{1}{J_m s^2 + c_m s} \quad (15)$$

Hence, various $Q(s)$ can be designed by $K(s)$ using (10). For example, if the controller is chosen as

$$K(s) = (J_m s + c_m)D \quad (16)$$

Then $Q(s)$ function has the form of

$$Q(s) = \frac{D}{s + D} \quad (17)$$

Therefore, it can be roughly said that the disturbances can be attenuated below the cutoff frequency ($\omega_c = D$ rad/s). Fig. 5 shows the whole control structure with RIC and feedback controller.

III. INDUSTRIAL EMULATOR/SERVO TRAINER

Industrial Plant Emulator (Model 220 produced by ECP)[8] is an equipment for teaching practical control of modern industrial field. This equipment has spindle drives, turntables, conveyors, machine tools, and automated assembly machines. Their adjustable dynamic parameters and ability to introduce or remove non-ideal properties in a controlled manner make it a perfect selection for industrial emulation of servo control.

1. System structure

Many experiments were conducted by using an industrial emulator in order to evaluate the performance of each controller which is already introduced in section II. Fig. 6 shows a frame structure of the industrial emulator.

Each consists of an electromechanical plant and a full complement

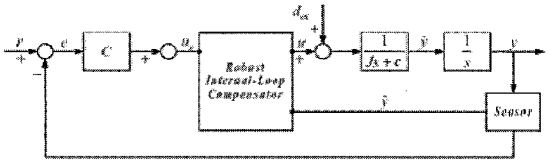

(a) 전체 제어시스템의 블록도.

(a) Block diagram of the overall control system.

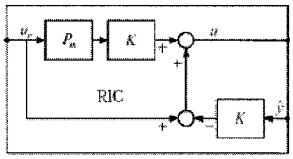

(b) RIC.

(b) RIC.

그림 5. 전체 제어 시스템과 RIC.

Fig. 5. Overall control system and RIC.

표 1. 질량 파라미터.

Table 1. Mass parameters.

Mass of brass weights[Kg]		Radius from center of plate[m]	
On drive disk : m_{wd}x4	0.8	On drive disk : r_{wd}	0.05
On load disk : m_{wl}x4	2.0	On load disk : r_{wl}	0.1

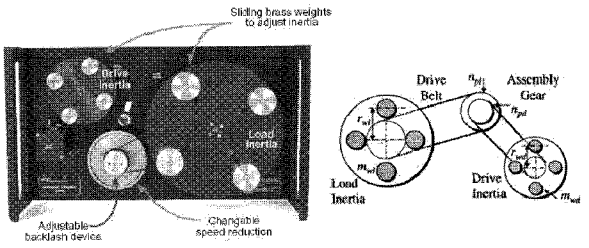

그림 6. Industrial 에뮬레이터(ECP 시스템 모델 220).

Fig. 6. Industrial emulator (ECP System model 220).

of control hardware and software. The industrial emulator consists of a multi-mass system connecting a drive inertia and load inertia via a driving belt through an assembly gear. In the Fig. 6, m_{wl} and m_{wd} are the mass of each brass element loaded on each plate, and r_{wl} and r_{wd} are the distances from the center of the plates. n_{pl} and n_{pd} are the number of teeth in the assembly gear. The inertia is determined by m_{wl} and r_{wl}, as well as m_{wd} and r_{wd}. In the experiment, m_{wl}: 0.5 Kg and m_{wd}: 0.2 Kg were used, with r_{wl}: 10 cm and r_{wd}: 5 cm. The assembly gear had n_{pl}: 36 and n_{pd}: 24. The mass parameters of industrial emulator were shown in Table 1.

A disturbance motor connects to the load disk via 4:1 speed reduction and is used to emulate viscous friction and disturbances at the plant output. A brake below the load disk may be used to apply Coulomb friction..

The drive inertia and load inertia each have a 16,000(counts/rev) encoder attached, and the drive inertia is directly connected to a brushless DC motor. A DSP board built in personal computer controls the industrial emulator. The input/output data to be observed are the drive torque [N-m] and the motor angular velocity [rad/s].

2. System identification

Before applying motion control theory, the inertia, gain, and damping ratio of the industrial emulator can be found indirectly by measuring their system characteristics. The following block diagram shown in Fig. 7 is used to identify system parameters.

The output/input transfer function is given by

$$\frac{\theta_1(s)}{r(s)} = \frac{k_p k_{hw}/J}{s^2 + (c + k_d k_{hw}/J)s + k_p k_{hw}/J} \quad (18)$$

Comparing (18) with the following second order system

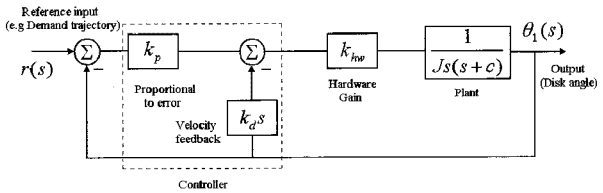

그림 7. 시스템 파라미터를 찾기 위한 블록도.

Fig. 7. Block diagram to find system parameters.

$$\frac{\theta_1(s)}{r(s)} = \frac{\omega_n^2}{s^2 + 2\varsigma\omega_n s + \omega_n^2} \tag{19}$$

Then, $\omega_n = \sqrt{\frac{k_p k_{hw}}{J}}$, $\varsigma = \frac{1}{2\omega_n}\left(c + \frac{k_d k_{hw}}{J}\right)$ are system *natural frequency* and *damping ratio*, respectively. When the plant viscous friction c is negligible compared to k_d, the damping ratio is

$$\varsigma \approx \frac{k_d k_{hw}}{2J\omega_n} = \frac{k_d k_{hw}}{2\sqrt{Jk_p k_{hw}}} \tag{20}$$

The hardware gain k_{hw} of the system consists of the product:

$$k_{hw} = k_c k_a k_t k_e k_s \tag{21}$$

where, k_c[DAC gain]=10V/32,768 DAC counts, k_a[Servo Amp. gain]=approx. 2[amp/V], k_t[Servo Motor Torque constant]=approx. 0.1[N-m/amp], k_e[Encoder gain]=16,000/2 π [pulses / radian], k_s[Controller Software gain]=32 [controller input /encoder pulses]. So, we can obtain the whole hardware gain of this system as k_{hw}=4.97.

3. Dynamics of rigid body

By inspection of Fig. 8, the overall drive train gear ratio, gr, is such that $\theta_1 = gr\theta_2$, i.e.

$$gr = \frac{r_l r_{p1}}{r_{p2} r_d} \tag{22}$$

We shall refer to the partial gear ratio between the idler pulley aszembly and the drive disk gr', i.e.:

$$gr' = r_{p1} / r_d \tag{23}$$

such that $\theta_l = gr'\theta_p$.

The drive inertia reflected to the load location, for example, is $J_d gr^2$. We may then express for Fig. 8:

$$J_d^* = J_d + J_p gr'^{-2} + J_l gr^{-2} \tag{24}$$

$$J_l^* = J_d gr^2 + J_p\left(\frac{gr}{gr'}\right)^2 + J_l \tag{25}$$

where J_d^* and J_l^* are the total inertias reflected to the drive and load respectively. Similarly for the friction coefficients it may be shown that

$$c_d^* = c_1 + c_2 gr^{-2} \tag{26}$$

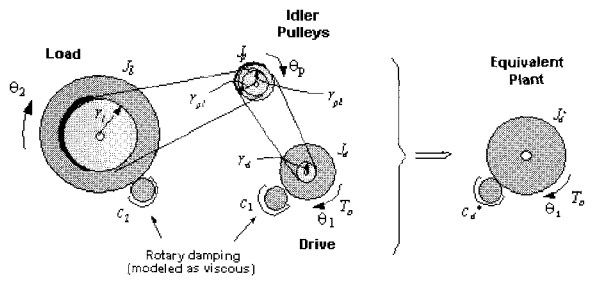

그림 8. Rigid body 플랜트 모델.

Fig. 8. Rigid body plant model.

$$c_l^* = c_1 gr^2 + c_2 \tag{27}$$

where c_d^* and c_l^* are the total reflected friction constants at the drive and load.

For many applications involving servo drives, non-ideal effects such as drive flexibility, backlash, static and kinetic friction, and other nonlinearities are sufficiently small, thus the plant may be modeled as a simple rigid body obeying Newton's second law. From Fig. 8, it can be expressed

$$J_d^*\ddot{\theta}_1 + c_d^*\dot{\theta}_1 = T_D \quad \text{or} \quad J_l^*\ddot{\theta}_2 + c_l^*\dot{\theta}_2 = grT_D \tag{28}$$

which has the Laplace transform:

$$\frac{\theta_1(s)}{T_D(s)} = \frac{1}{s(J_d^* s + c_d^*)}, \quad \frac{\theta_2(s)}{T_D(s)} = \frac{gr}{s(J_l^* s + c_l^*)} \tag{29}$$

If the friction is neglected these equations can be further reduced to

$$J_d^*\ddot{\theta}_1 = T_D, \quad J_l^*\ddot{\theta}_2 = grT_D \tag{30}$$

$$\frac{\theta_1(s)}{T_D(s)} = \frac{1}{J_d^* s^2}, \quad \frac{\theta_2(s)}{T_D(s)} = \frac{gr}{J_l^* s^2} \tag{31}$$

4. Flexible drive dynamics

A model of the emulator plant with flexibility in the drive train is shown in Fig. 9a. Using the free body diagram of Fig. 9b and summing torques acting on J_l, following equations can be obtained by Newton's second law (in its rotational form)

$$(F_1 - F_2)r_l - c_2\dot{\theta}_2 = J_l\ddot{\theta}_2 \tag{32}$$

$$\text{or} \quad J_l\ddot{\theta}_2 + c_2\dot{\theta}_2 + 2k_L\left(r_l\theta_2 - r_{p2}\theta_p\right)r_l = 0 \tag{33}$$

By defining a torsional (or rotary) spring constant

$$k = 2k_L r_l^2 \tag{34}$$

Finally, the desired equations of motion are obtained in two coordinates:

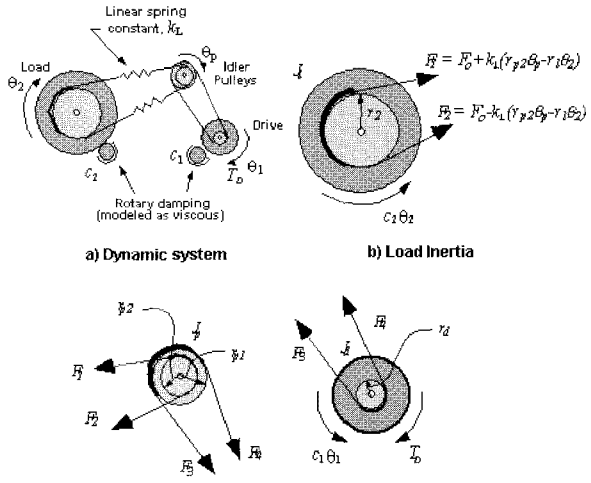

그림 9. Flexible body 플랜트 모델.

Fig. 9. Flexible body plant model.

$$J_d^*\ddot{\theta}_1 + c_1\dot{\theta}_1 + k\left(gr^{-2}\theta_1 - gr^{-1}\theta_2\right) = T_D \tag{35}$$

$$J_l\ddot{\theta}_2 + c_2\dot{\theta}_2 + k\left(\theta_2 - gr^{-1}\theta_1\right) = 0 \tag{36}$$

Converting to state space representation, then

$$\begin{aligned} \dot{X} &= AX + BT(t) \\ Y &= CX \end{aligned} \tag{37}$$

where:

$$X = \begin{bmatrix} \theta_1 \\ \dot{\theta}_1 \\ \theta_2 \\ \dot{\theta}_2 \end{bmatrix},$$

$$A = \begin{bmatrix} 0 & 1 & 0 & 0 \\ -kgr^{-2}/J_d^* & -c_1/J_d^* & kgr^{-1}/J_d^* & 0 \\ 0 & 0 & 0 & 1 \\ kgr^{-1}/J_l & 0 & -k/J_l & -c_2/J_l \end{bmatrix}$$

$$B = \begin{bmatrix} 0 \\ 1/J_d^* \\ 0 \\ 0 \end{bmatrix}, \quad C = \begin{bmatrix} C_1 & 0 & 0 & 0 \\ 0 & C_2 & 0 & 0 \\ 0 & 0 & C_3 & 0 \\ 0 & 0 & 0 & C_4 \end{bmatrix}$$

and $C_i = 1$ (i=1,2,3,4) when X_i is an output and equals 0 otherwise. From the Laplace transform we have:

$$\frac{\theta_1(s)}{T_D(s)} = \frac{J_l s^2 + c_2 s + k}{D(s)} \tag{38}$$

$$\frac{\theta_2(s)}{T_D(s)} = \frac{k/gr}{D(s)} \tag{39}$$

where

$$\begin{aligned} D(s) = {} & J_d^* J_l s^4 + \left(J_d^* c_2 + J_l c_1\right)s^3 \\ & + \left(J_d^* k + J_l gr^{-2}k + c_1 c_2\right)s^2 \\ & + \left(c_1 k + c_2 gr^{-2}k\right)s \end{aligned} \tag{40}$$

In systems where the flexible element contains a significant fraction of the plant damping, it may be useful to include this damping in the plant model. Such damping may arise is when the flexible element is a drive belt. The inclusion of the coupled friction is not necessary in many practical applications. It does render better agreement between simulation and system test results.

IV. EXPERIMENTS

The industrial emulator described in previous section is used in designing each controller. The PID, LQR and RIC controllers are used for rigid and flexible body to compare performance of the command tracking and disturbance attenuation. The initial conditions of each controller are shown in Table 2.

The experimental setup includes a PC based control platform and a brushless DC servo system shown in Fig. 6. The disturbance signal d is applied to the load disk via a 4:1 speed reduction from a disturbance motor.

표 2. 각 제어기에서 사용한 초기조건과 이득.

Table 2. Initial conditions and gains used each controller.

	PID	LQR	RIC
Rigid body	K_p=0.4143 K_i=0.4 K_d=0.0208	$Q = \begin{bmatrix} 1 & 0 & 0 \\ 0 & 0 & 0 \\ 0 & 0 & 0 \end{bmatrix}$ R=1.0	k_p=0.4143 k_d=0.0248 J_m=0.08 c_m=0.04 D=1~10
Flexible body	K_p=0.2582 K_i=0.56 K_d=0.0164	$Q = \begin{bmatrix} 0 & 0 & 0 & 0 \\ 0 & 0 & 0 & 0 \\ 0 & 0 & 1 & 0 \\ 0 & 0 & 0 & 0 \end{bmatrix}$ R=1.0	k_p=0.2582 k_d=0.0178 J_m=0.02 c_m=0.06 D=1~10

1. Control of rigid body

In this comparative experiment, we use PID control as a reference to compare the performance of disturbance attenuation. All of experiments use same reference command and same disturbance.

In RIC structure, $K(s)$ is chosen as

$$K(s) = \frac{1}{P_m(s)}\left[\frac{D(s)}{s}\right] = \left(J_m(s) + c_m\right)D(s) \tag{41}$$

Then the Q-filter of DOB has the form of

$$Q(s) = \frac{D(s)}{s + D(s)} \tag{42}$$

And the external-loop controller is represented by PD controller with K_p=0.4143, K_d=0.0208.

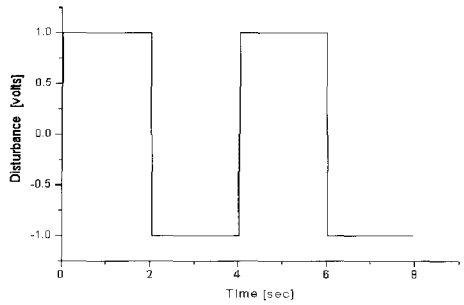

(a) 스텝 외란.

(a) step disturbance.

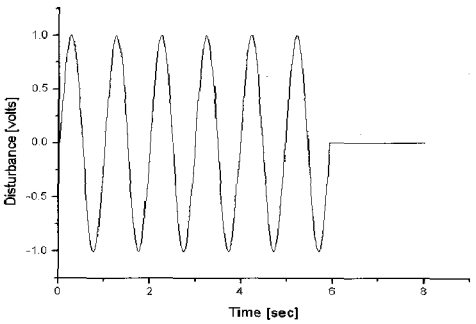

(b) 정현파 외란.

(b) sinusoidal disturbance.

그림 10. 외란의 형태.

Fig. 10. The shape of disturbance.

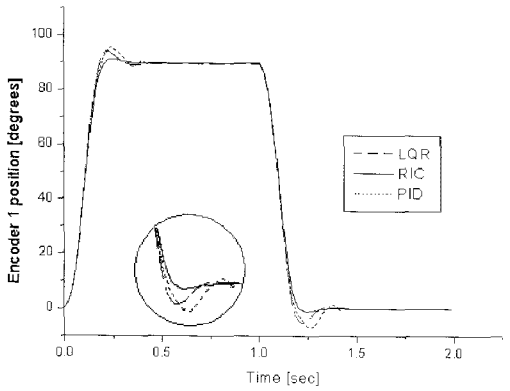

그림 11. 외란이 없을 때의 각 제어기의 스텝 응답.

Fig. 11. Step response for each controller without disturbance.

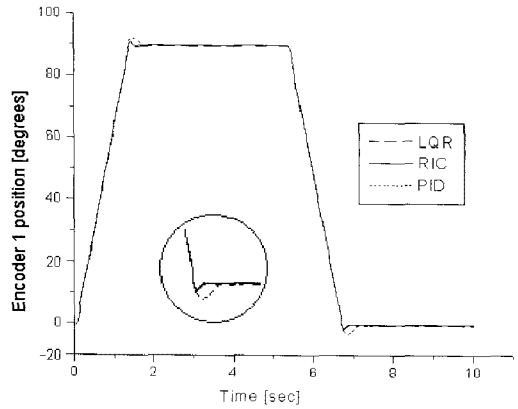

그림 12. 외란이 없을 때의 각 제어기의 사다리꼴 응답.

Fig. 12. Trapezoidal responses for each controller without disturbance.

The practical plant parameters were calculated by using the rigid structure of section III. It can be represented as

$$P(s)=\frac{k_{hw}}{J_d^* s^2+c_d^* s}=\frac{4.97}{0.0042s^2+0.0071s} \tag{43}$$

The reference nominal model of the system was selected as

$$P(s)=\frac{k_{hw}}{J_m s^2+c_m s}=\frac{5.0}{0.005s^2 0.008s} \tag{44}$$

Two kinds of disturbance signal, step or sinusoidal form shown in Fig. 10 are applied to load disk. Maximum disturbance is 1 *volt* (≈ 0.2 *N-m*). Two kinds of reference command, step and trapezoidal profile, are used. Maximum reference command angle is 4000 *counts*(=90 *degrees*).

Fig. 11 and Fig. 12 depict the step responses and trapezoidal responses of each controller when the disturbance is not applied. The rise time for step command is about 0.11 sec. From the results, the trapezoidal responses have better performance than step responses. Since the motion control system usually adopts trapezoidal profile, these three controllers can be applied into motion control system from experimental results. The response of RIC controller has the best performance.

Fig. 13, Fig. 14 and Fig. 15 show the disturbance attenuation property of step responses and trapezoidal responses of each controller in the presence of step disturbances. For step command, RIC has the

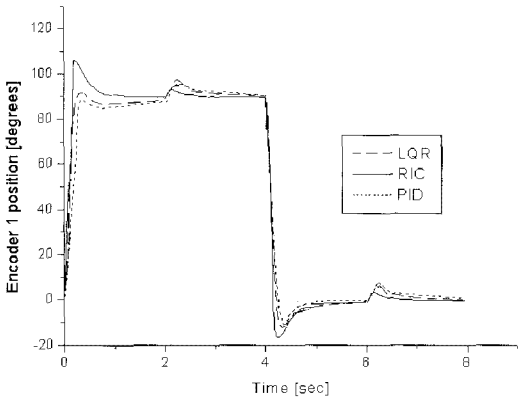

그림 13. 스텝 외란 인가시의 각 제어기의 스텝 응답.

Fig. 13. Step response for each controller in the presence of step disturbance.

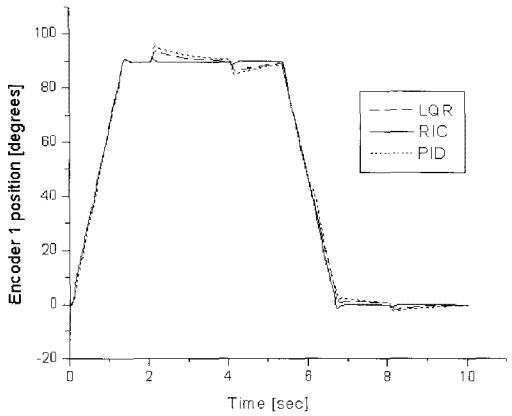

그림 14. 스텝 외란 인가시의 사다리꼴 응답.

Fig. 14. Trapezoidal responses in the presence of step distur-bance.

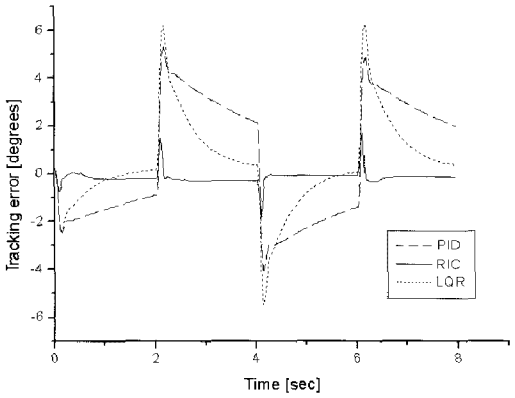

그림 15. 스텝 외란에 대한 PID, LQR, RIC의 추종오차(사다리꼴 경우).

Fig. 15. The tracking error of PID, LQR and RIC with step disturbance(trapezoidal case).

best performance in view of attenuation property of disturbance, even though larger overshoot occurs in the transient response. In case of trapezoidal responses, the RIC has the much better performance than LQR, and PID. Fig. 16 shows only the tracking errors of each controller. In case of RIC, when the step disturbance is applied, the spike-like error occurs. But the error of RIC caused by disturbance is attenuated very quickly unlikely the error of PID case, which decreases very slowly.

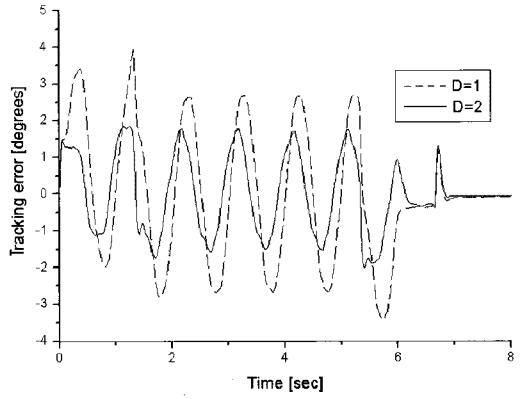

그림 16. 정현파 외란 인가시의 D의 변화에 대한 RIC의 추종 오차 비교.

Fig. 16. Comparison of tracking error of RIC vs. D in the presence of sinusoidal disturbance.

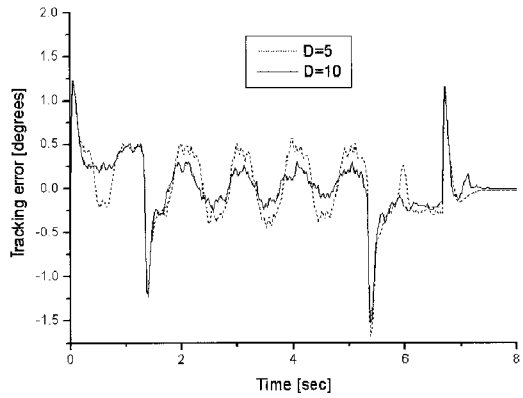

그림 17. 정현파 외란 인가시의 D의 변화에 대한 RIC의 추종 오차 비교.

Fig. 17. Comparison of tracking error of RIC vs. D in the pres-ence of sinusoidal disturbance.

Specifically, when D is large enough or the system is operated in low-frequency range, we can predict that if D is increased by N times, the error will be reduced to its $1/N$, approximately. In experiments, D is not polynomial, but constant. Fig. 16 and Fig. 17 show the tracking errors of trapezoidal command for various D when the sinusoidal disturbance is applied. If D is increased from 1 to 10, the tracking error is reduced from 6 degrees to 0.6 degrees. Consequently, it can be seen that the performance variation governed by the gain D of RIC compensator.

Now the experiment to compensate the friction is performed to consider affection by it. Friction exists to some extent in all practical mechanical systems. It may be modeled as being a combination of static, Coulomb (kinetic), and viscous types. Coulomb and static friction magnitude are often greater than viscous friction and deteriorate the control design problem in that they are nonlinear. In small amounts they may actually help to stabilize a system, but generally are deleterious to tracking and regulation performance. To apply Coulomb friction, place a single $0.5Kg$ brass weight at r=10 *cm* on the load disk and adjust the clamp such that the load disk rotates very slowly (or rotation is initiated by very slight downward force on the weight). Approximately 0.5 *N-m* of friction torque is applied to the

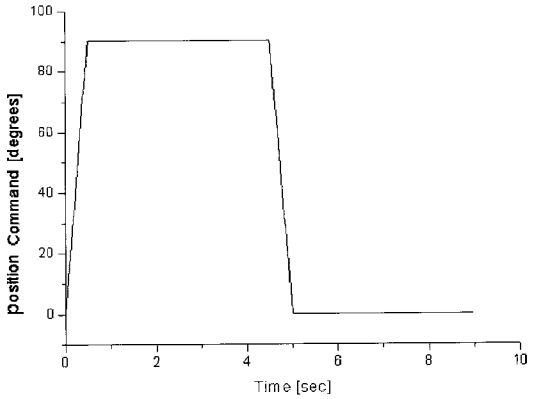

그림 18. 마찰실험에서의 기준입력 프로파일.

Fig. 18. Reference command profile used in friction experiment.

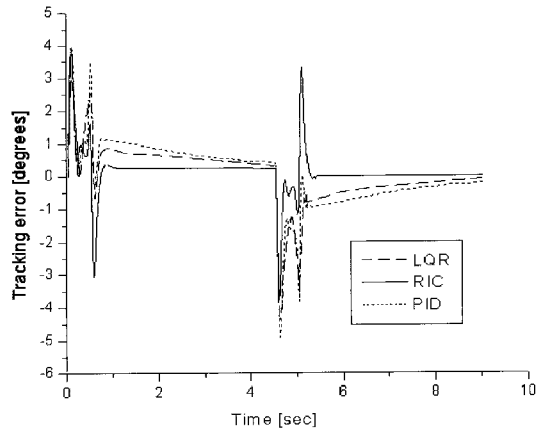

그림 19. 마찰 인가시의 추종오차.

Fig. 19. Tracking error in the presence of friction.

load shaft when it rotates. Fig. 18 shows the reference position profile, *Distance*=4000 *counts*, *Velocity*=8000 *counts/sec*, *Dwell time*=4[*sec*]. Fig. 19 shows the tracking errors of each controller in the presence of Coulomb friction. Spike-like tracking errors occur in the time of discontinuous motion for each controller. RIC has the shortest stabilizing property to attenuate friction, even though the spike-like error occurs. But it is shown that the spike-like error does not occur in discontinuous motion from Fig. 14 and Fig. 15, the results without friction. It is shown that the friction is main factor to occur spike-like error..

2. Control of flexible plant

In this section, we try to do experiment for the plant with drive flexibility. The belt of industrial emulator is replaced by flexible one. The model of our plant belongs to a class having two degrees of freedom(*DOF*) corresponding to normal modes of oscillation (actually one oscillatory and one rigid body mode in our case) and hence is of fourth order. The block diagrams of the system for time and Laplace domain analyses are shown in Fig. 20 that gives details of the location of k_{hw} gain elements in the signal flow. The signals θ_{1e} and θ_{2e} are the respective angle measurements in encoder counts.

2.1 PID control

The PID control is conducted for the 2-disk flexible system where the feedback signal, θ_1 is of the drive disk. But the results figure shows load disk angle θ_2. The PID responses are shown by dotted line in Fig.

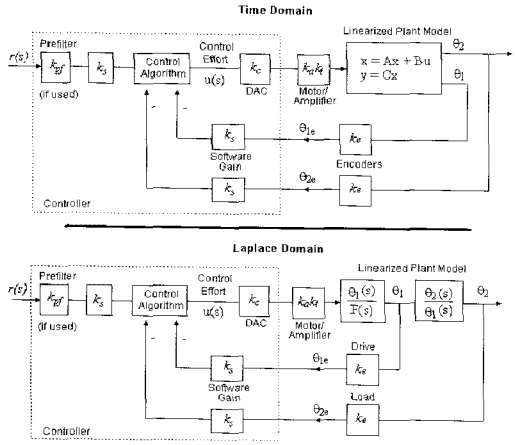

그림 20. 2 DOF 제어를 위한 블록도(SIMO).

Fig. 20. Block diagram for 2 DOF control (SIMO).

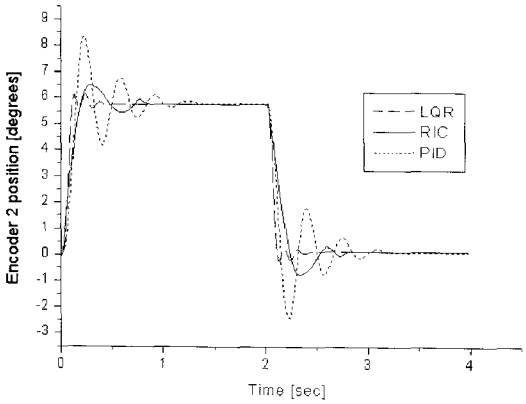

그림 21. Flexible body에 대한 각 제어기의 스텝 응답.

Fig. 21. Step responses of each controller for flexible body.

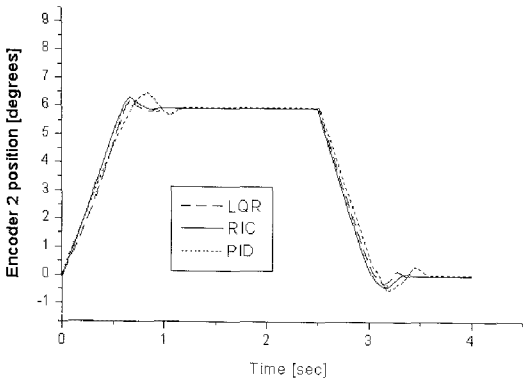

그림 22. Flexible body에 대한 각 제어기의 사다리꼴 응답.

Fig. 22. Trapezoidal responses of each controller for flexible body.

21(step command) and Fig. 22(trapezoidal command).

2.2 RIC control

In RIC experiment, the same structure as rigid body case is used. The only encoder 2 signal is used as feedback signal. The experiment results are shown by solid line in the Fig. 21 and Fig. 22.

2.3 Full state feedback LQR control

The states chosen are the disk angles and rates according to the model of section III, the feedback encoders measure the angular outputs. The encoders are backwards differentiated in the controller to provide a rate measurement and hence the four defined states are available for control. The state feedback controller was designed with weight values: $R = 1.0$. In the block diagrams of Fig. 20, the prefilter gain K_{pf} must be set equal to $grK_1 + K_3$. The LQR experiment results are shown by dash lines in the Fig. 21 and Fig. 22. LQR design often provides well-behaved, relatively high performance controllers for servo equipment with drive flexibility. It may be readily implemented whenever full state feedback is available.

V. CONCLUSION

Through the motion control experiments using Industrial Emulator, the performance comparison of three kinds of controllers such as PID, RIC and LQR was carried out in view of the command tracking and disturbance rejection property. It was shown that RIC has the best performance in tracking and disturbance rejection for rigid body plant, but has big overshoot in case of step command. On the other hand, LQR with full state feedback has the best tracking property for the flexible body.

The design procedure of PID controller is very simple, but the performance is not good as compared with others. The design procedure of LQR in the state space is the most complicated even though it is the most advanced modern controller. The additional state observer should be augmented in order to estimate disturbance, which makes the control system more complex. The design process of RIC lies between PID and LQR in view of complexity of design procedure. Considering all these aspects, the RIC might be suggested as high precision controller for motion control system.

REFERENCES

[1] D. Lunberger, "Observers for multivariable systems," *IEEE Trans. Automatic Control*, 11, pp. 190-197, 1966.

[2] B. K. Kim and W. K. Chung, "Advanced Disturbance Observer Design for Mechanical Positioning Systems," *IEEE Trans. on Industrial Electronics*, vol. 50, no. 6, pp. 1207-1216, 2003.

[3] L. X. Li and Bin Yao, "Adaptive Robust Precision Motion Control of Linear Motors with Negligible Electrical Dynamics: Theory and Experiments," *IEEE/ASME Trans. on Mechatronics*, vol. 6, no. 4, pp. 444-452, 2001.

[4] Z. Gao, S. Hu and Fangjun Jiang, "A Novel Motion Control Design Approach Based On Active Disturbance Rejection," *Proceeding of the 40th IEEE Conference on Decision and Control*, pp. 4877-4822, 2001.

[5] T. Ohmae, Matsuda, M. Kanno and K. Saito, "A Microprocessor-Based Motor Speed Regulator Using Fast-Response State Observer for Reduction of Torsional Vibration," *IEEE Trans. Ind. Applicat.*, vol. 1A-23, no. 5, Sep. 1987.

[6] H. S. Lee and M. Tomizuka, "Robust Motion Controller Design for High Accuracy Positioning Systems," *IEEE Trans. Ind. Electron.*, vol. 43, pp. 48-55, 1996.

[7] B. K. Kim and W. K. Chung, "Performance Tuning of Robust Motion Controllers for High-Accuracy Positioning Systems," *IEEE/ASME Trans. on Mechatronics*, vol. 7, no. 4, pp. 500-514, 2002.

[8] *Manual for Model 220 Industrial Emulator/Servo Trainer, Educational Control Products*, 5725 Ostin Avenue, Woodland Hills, CA 91367, 1995.

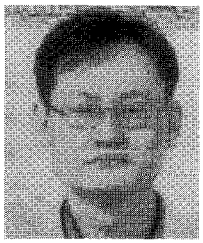

Seung Hyun Jung

He received B.S. and M.S. degrees in Electronic Engineering from Yeungnam University, Gyeongsan, Korea, in 1995 and 1998, respectively. He is currently Ph.D. degree student in Dept. of Electronic Engineering, Yeungnam University. From 2000 to 2002 he worked as a Assistant Engineer at LG electronics . He is currently Automation Technology Senior Researcher of the Korea Textile Machinery Research Institute, Gyeongsan, Korea. His current research interests are high-precision motion control, nonlinear control, neurofuzzy control.

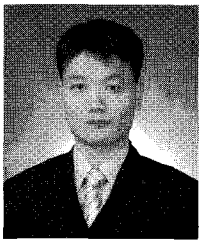

Chang Wook Han

He received the B.S., M.S., and Ph.D. degrees in Electronic Engineering from Yeungnam University, Gyongsan, Korea in 1994, 1996, and 2002, respectively. From 1996 to 1997, he worked as an engineer at Hyundai Heavy Industries Co., Ltd. During 2002-2003, he was a Post- doctoral Fellow in the Department of Electrical and Computer Engineering at the University of Alberta, Canada. From 2004 to 2007, he worked as a guest professor at School of Electrical Engineering and Computer Science, Yeungnam University, Korea. He joined the faculty of the Department of Electrical Engineering, Dong-Eui University, Busan, Korea in 2008, where he has been a full time lecturer. His research interests include fuzzy-neural networks, intelligent control, computational intelligence and its applications.

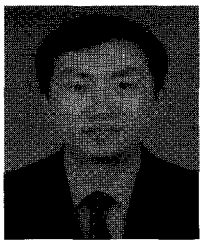

Jun Wang

Wang Jun received the B.S. degree in Mechanical and production engineering from the University of Electronic Science and Technology of China, in 1995, and the M.S. degrees in Electronic engineering from Yeungnam University, Korea, in 2005. From 1995 to 2003 and 2005 to 2008, he was a teacher in the School of Electronic Engineering, the University of Electronic Science and Technology of China. His research interests include control of high-speed systems, high-speed sampling data systems, digital signal processing.

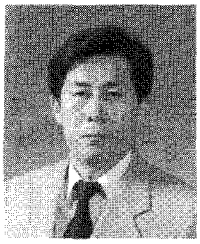

Jung-Il Park

He received the B.S. degree in Electronic Engineering from Kyoungbuk National University, Daegu, Korea in 1981, and the M.S. and Ph.D. degrees in Electronic Engineering from Seoul National University, Seoul, Korea, in 1983 and 1989, respectively. From 1989 to 1992 he worked as a Senior Engineer at Samsung Advanced Institute of Technology. He joined the faculty of the school of Electrical Engineering and Computer Science, Yeungnam University, Gyoungsan, Korea in 1992, where he has been a professor since 2003. His current research interests are neural-based intelligent control, high-precision motion control, networked control system..